Dalton Transactions

An international journal of inorganic chemistry
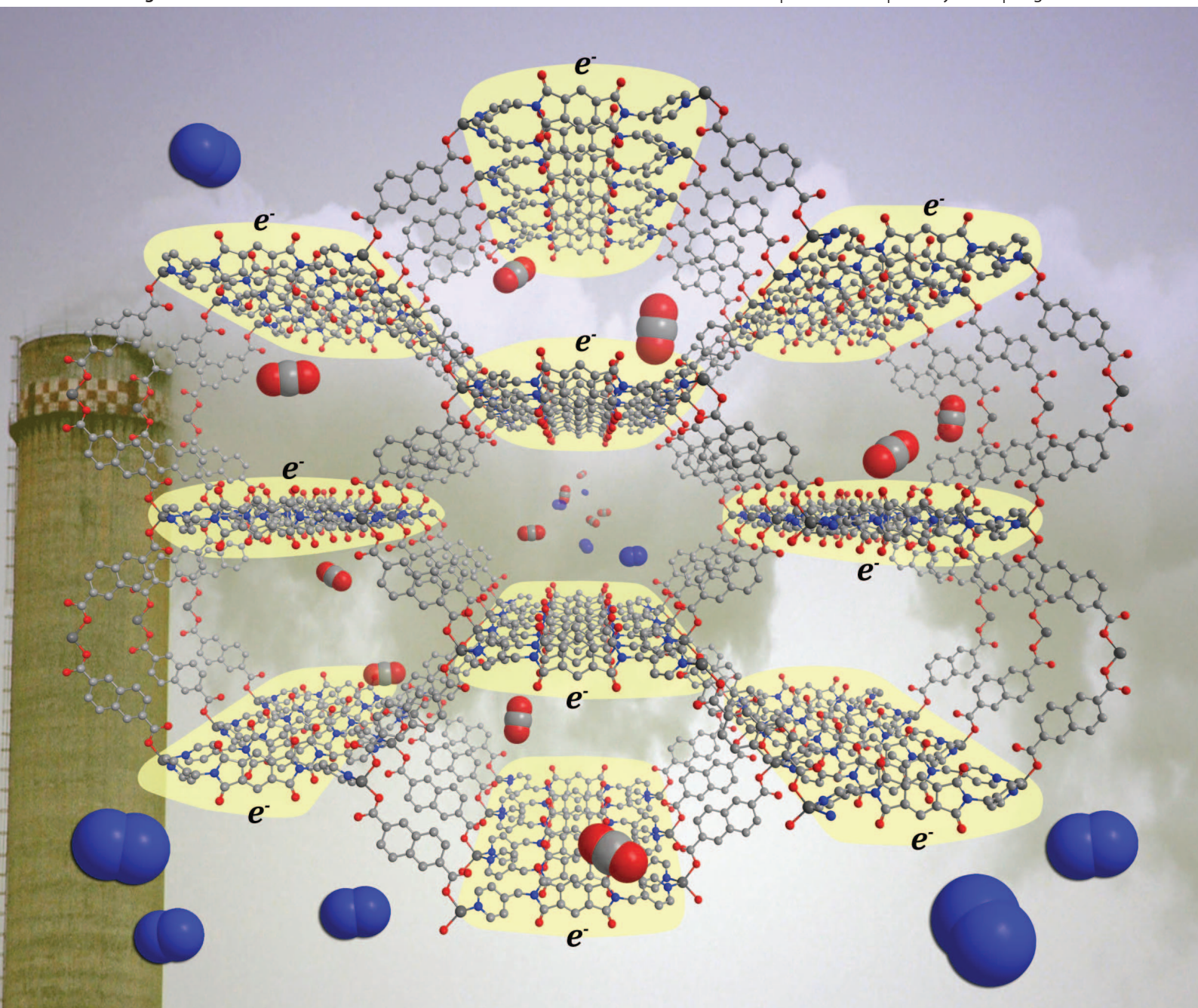
RSCPublishing

COVER ARTICLE
D'Alessandro *et al.*
Enhancing selective CO$_2$ adsorption *via* chemical reduction of a redox-active
metal–organic framework

Enhancing selective CO_2 adsorption *via* chemical reduction of a redox-active metal–organic framework†

Chanel F. Leong,[a] Thomas B. Faust,[a] Peter Turner,[a] Pavel M. Usov,[a] Cameron J. Kepert,[a] Ravichandar Babarao,[b] Aaron W. Thornton[b] and Deanna M. D'Alessandro*[a]

A new microporous framework, Zn(NDC)(DPMBI) (where NDC = 2,7-naphthalene dicarboxylate and DPMBI = *N*,*N*′-di-(4-pyridylmethyl)-1,2,4,5-benzenetetracarboxydiimide), containing the redox-active benzenetetracarboxydiimide (also known as pyromellitic diimide) ligand core has been crystallographically characterised and exhibits a BET surface area of 608.2 ± 0.7 m^2 g^{-1}. The crystallinity of the material is retained upon chemical reduction with sodium naphthalenide (NaNp), which generates the monoradical anion of the pyromellitic diimide ligand in the framework Zn(NDC)(DPMBI)·Na$_x$ (where x represents the molar Na$^+$/Zn^{2+} ratio of 0.109, 0.233, 0.367 and 0.378 from ICP-AES), as determined by EPR, solid state Vis-NIR spectroelectrochemistry and UV-Vis-NIR spectroscopy. The CO_2 uptake in the reduced materials relative to the neutral framework is enhanced up to a Na$^+$/Zn^{2+} molar ratio of 0.367; however, beyond this concentration the surface area and CO_2 uptake decrease due to pore obstruction. The CO_2 isosteric heat of adsorption ($|Q_{st}|$) and CO_2/N_2 selectivity (S), obtained from pure gas adsorption isotherms and Ideal Adsorbed Solution Theory (IAST) calculations, are also maximised relative to the neutral framework at this concentration of the alkali metal counter-ion. The observed enhancement in the CO_2 uptake, selectivity and isoteric heat of adsorption has been attributed to stronger interactions between CO_2 and both the radical DPMBI ligand backbone and the occluded Na$^+$ ions.

Introduction

Metal–organic frameworks (MOFs) have been the subject of significant interest due to their promise in the fields of gas separation and storage, sensing, catalysis, guest exchange and drug delivery.[1] In addition to the highly porous nature of MOFs, functionalisation of their internal surfaces has been exploited to tune their properties for preferential gas adsorption. A number of prospective frameworks requiring mild regeneration conditions have been reported which are selective for CO_2 adsorption over N_2 from the post-combustion flue streams of coal-fired power stations (a typical flue stream contains 0.15 bar CO_2, 0.75 bar N_2 and 0.10 bar impurities).[2,3]

Recent studies have been conducted into the incorporation of redox activity into MOFs as a strategy towards enhancing selective gas adsorption, with particular attention focused on H_2 storage,[4–6] CO_2/CH_4 separation[7] and CO_2 adsorption.[8] The enhancement in selective gas adsorption upon chemical reduction of MOFs such as Zn_2(NDC)$_2$(DPNI) incorporating the *N*,*N*′-di(4-pyridyl)-1,4,5,8-naphthalenetetracarboxydiimide (DPNI) ligand has been attributed to two effects, including (i) the improved electrostatic interactions between the quadrupole moment of CO_2 and the charged framework components, and (ii) the favourable displacement of catenated frameworks *via* doping with alkali cations.[7]

The present work reports the synthesis of a novel three-dimensional framework Zn(NDC)(DPMBI) that incorporates the flexible redox-active ligand *N*,*N*′-di-(4-pyridylmethyl)-1,2,4,5-benzenetetracarboxydiimide (DPMBI). The benzenetetracarboxydiimide (also known as pyromellitic diimide) ligand core is capable of two reversible reduction processes to form the monoradical anion and dianion, respectively.[9,10] The modification of the pyromellitic diimide moiety to accommodate pendant pyridyls capable of metal ligation enables the incorporation of this electronically interesting functionality into a three-dimensional structure.[11,12] Systematic chemical reductions of the framework with sodium naphthalenide (NaNp) enable the formation of the anionic forms of the pyromellitic diimide core as well as the subsequent intercalation of

[a] School of Chemistry, The University of Sydney, New South Wales 2006, Australia. E-mail: deanna@chem.usyd.edu.au; Fax: +61 (2) 9351 3329; Tel: +61 (2) 9351 3777
[b] Materials Science and Engineering Division, Commonwealth Scientific and Industrial Research Organisation (CSIRO), Clayton, Victoria 3168, Australia

†Electronic supplementary information (ESI) available: Additional crystallographic, TGA, IR, PXRD, EPR, spectroelectrochemical, gas adsorption and selectivity data. CCDC 918611. For ESI and crystallographic data in CIF or other electronic format see DOI: 10.1039/c3dt00083d

Na$^+$ ions. The applicability of the material for post-combustion CO_2/N_2 separation in its different electronic states is assessed by evaluating CO_2 isosteric heat of adsorption ($|Q_{st}|$) and selectivity (S), obtained *via* pure gas adsorption isotherms and Ideal Adsorbed Solution Theory (IAST) calculations. The utility of a recently reported technique for solid state Vis-NIR spectroelectrochemistry on MOFs[13] is demonstrated by the application of the method to characterise the spectra of the Zn(NDC)(DPMBI) framework as a function of its redox state.

Results and discussion

Structure of Zn(NDC)(DPMBI)·2DMF

The framework Zn(NDC)(DPMBI)·2DMF crystallises in the orthorhombic space group *Pbcn*(#60) with cell parameters a = 25.9151(1), b = 14.1744(1) and c = 20.6042(1) Å (refer to Table S1, ESI† for further information). Each tetrahedrally-coordinated Zn^{2+} centre is connected to two NDC ligands (carboxylato-κ^1*O*) and two DPMBI ligands (through the pyridyl nitrogen; see Fig. 1), with bridging through these ligands yielding a 3D diamondoid-type coordination framework. Four such networks interpenetrate within the structure. The unit cell possesses four columns of stacked aromatic units which run along the *b* axis, each consisting of alternating DPMBI and NDC moieties. Only three of the networks are represented in each column. For clarity, the separate networks are designated **A**, **B**, **C** and **D**. Each stack can be assigned a label (**i**, **ii**, **iii** and **iv**) according to the identity of its DPMBI unit, since these are unique to each column. Column **i** consists of DPMBI units from network **A** and NDC units from networks **B** and **C**, and has the stacking arrangement **A B A C**. Column **ii** has the stacking arrangement **B A B D**, while columns **iii** and **iv** have arrangements **C A C D** and **D B D C**, respectively. The stacking distance (calculated by measuring the distance between centroids defining the core of the C$_6$ ring of DPMBI and the centre of bond C(26)–C(28)) alternates between 3.583(1) and 3.511(1) Å.

The π–π* stacking interactions that arise from (or more likely drive) the high degree of catenation contribute towards framework stabilisation at the expense of porosity.[14] Channels occupied by DMF molecules run between the columns along the *b* axis. There do not appear to be any hydrogen bonding interactions between the solvent molecules and the framework. TGA revealed a 15% weight loss due to solvent which was in reasonable agreement with the DMF content of the crystal structure (17.7% DMF by mass). Calculation of the void volume after removal of the DMF molecules revealed a pore accessible volume which was 30.7% of the unit cell volume as determined from PLATON (by defining regions >1.2 Å from the nearest van der Waals surface using a 0.2 Å grid). A pore size analysis of the quadruply interpenetrated structure revealed that the diameter of the one dimensional pores lie in the narrow range of 3.35–4.55 Å, as calculated using the RASPA package (ESI†).[15]
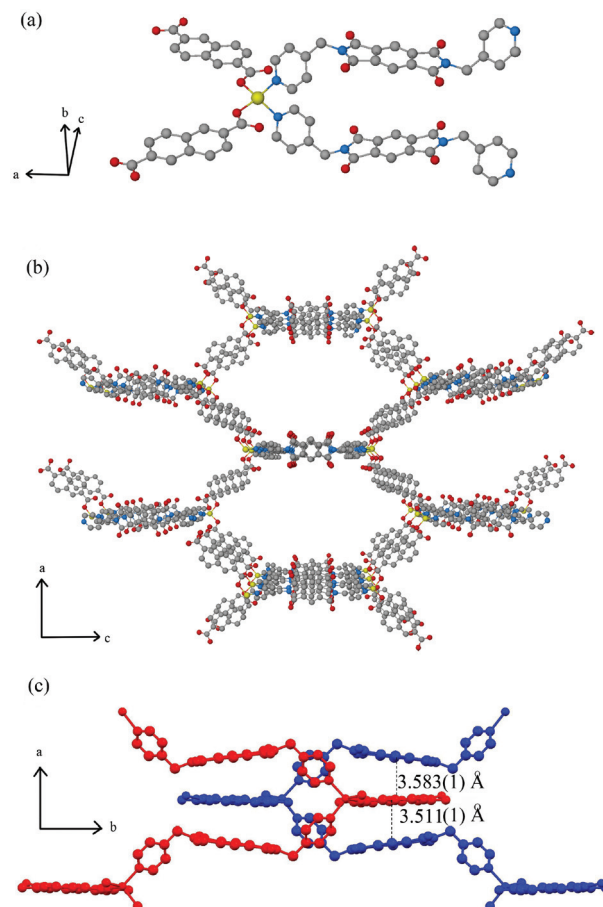

Fig. 1 Ball-and-stick representations of (a) the tetrahedrally-coordinated Zn^{2+} centre and (b) the extended crystal structure of a single Zn(NDC)(DPMBI) framework viewed down the *b* axis where hydrogen atoms, DMF molecules and three of the four interpenetrated frameworks are omitted for clarity (colour scheme: zinc, yellow; carbon, grey; oxygen, red; nitrogen, blue). (c) Diagram of two catenated frameworks (blue and red) showing distances between the stacked DPMBI-NDC-DPMBI layers.

Le Bail refinement of the PXRD pattern obtained from a bulk sample of the as-synthesised Zn(NDC)(DPMBI) framework at 298 K was in good agreement with the single crystal data, whereby the fitted unit cell parameters of a = 25.893(7), b = 14.470(4) and c = 20.672(7) Å are very similar to those determined from the single crystal X-ray measurement at 150 K.

To facilitate desolvation of the bulk material, DMF was exchanged for methanol *via* a Soxhlet washing procedure: the complete removal of DMF was evidenced by the absence of the characteristic carbonyl stretching frequency, ν(C=O), at 1669 cm^{-1} in the IR spectrum of Zn(NDC)(DPMBI) after solvent exchange (ESI†). Subsequent evacuation of the material at 110 °C under vacuum[6] resulted in a colour change from pale yellow to off-white which was reversible upon re-exposure to air. The structural integrity of Zn(NDC)(DPMBI) was retained throughout the washing and activation procedure as confirmed by PXRD (ESI†). The minor variations in the positions and intensities of the diffraction peaks for the desorbed material are indicative of a small degree of structural

distortion upon desolvation, as may be reasonably expected for the four-fold interpenetrated network incorporating the DPMBI ligand which itself exhibits a small degree of flexibility due to the methylene linkers. Le Bail refinements on the activated framework yielded unit cell parameters of $a = 25.652(4)$, $b = 14.112(2)$ and $c = 19.024(3)$ Å, which are smaller than those determined for the bulk as-synthesised sample at 298 K. This reduction in the unit cell dimensions is reasonable considering the closer proximities of the catenated frameworks as solvent molecules are removed from the structure.

Electrochemistry and chemical reduction of Zn(NDC)(DPMBI)

Solid state electrochemical measurements on Zn(NDC)-(DPMBI) revealed two reversible reduction processes at −1.27 and −1.92 V $vs.$ Fc^0/Fc^+ which can be assigned to the formation of the monoradical and dianion forms of DPMBI, respectively (Fig. 2).[16] The electrochemical behaviour is similar to that reported previously in the literature for compounds containing ligands based on the pyromellitic diimide core, which indicates that the redox processes in the framework are localised on this redox-active ligand.[9]

Since NaNp is a single-electron reductant, with a reduction potential more cathodic than that required for DPMBI radical formation (−3.10 V $vs.$ Fc^0/Fc^+ in THF[17]), one and two electron reductions of Zn(NDC)(DPMBI) were conducted using stoichiometric additions of the reductant. The naphthalenide radical is subsequently oxidised to naphthalene following the reduction of the framework under an inert atmosphere.

Due to the high degree of interpenetration and hence the small pore space in Zn(NDC)(DPMBI), chemical reductions were carried out via the addition of the reducing agent in THF followed by copious washing with THF to ensure the complete removal of weakly adsorbed naphthalene. Na$^+$ ions accumulate in the pores upon formation of the DPMBI radical anion. The counter-ion content was determined by solution-state ICP-AES, where the molar Na$^+$/Zn^{2+} ratios were found to be 0.109, 0.233,
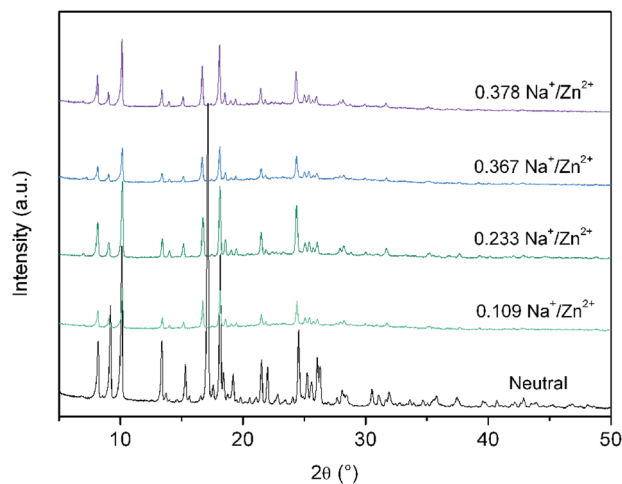

Fig. 3 Overlay of the capillary PXRD patterns for the neutral Zn(NDC)(DPMBI) framework and its reduced species.

0.367 and 0.378 for Zn(NDC)(DPMBI) which was reduced using 0.5, 1, 1.5 and 2 equivalents of NaNp, respectively. The retention of framework crystallinity was confirmed via capillary PXRD measurements of each of the reduced Zn(NDC)(DPMBI) species (Fig. 3). Le Bail refinements of the PXRD patterns for the reduced frameworks revealed that each pattern could be fitted using a single phase refinement, with unit cell parameters that were very similar to those determined for the neutral framework (ESI†).

The incomplete chemical reduction of the frameworks and the correspondingly low concentrations of Na$^+$ that are incorporated may be attributed to slow diffusion of NaNp through the highly interpenetrated structure. This suggests that a majority of the redox activity occurs at the surface of the crystallites, rather than being homogeneously distributed throughout the pores of the framework.

Chemical reduction of Zn(NDC)(DPMBI) was accompanied by distinct colour changes from light yellow in the neutral material to green and purple (Fig. 4). A similar observation was reported previously for the one-electron reduction of
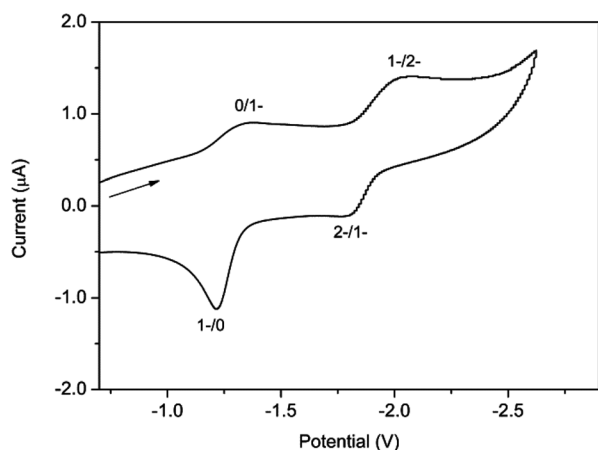

Fig. 2 Solid state cyclic voltammogram of Zn(NDC)(DPMBI) in 0.01 M [n-Bu$_4$N]-PF$_6$/CH$_3$CN at a scan rate of 100 mV s^{-1}. Potentials are referenced to Fc^0/Fc$^+$ and the arrow indicates the direction of the forward scan.
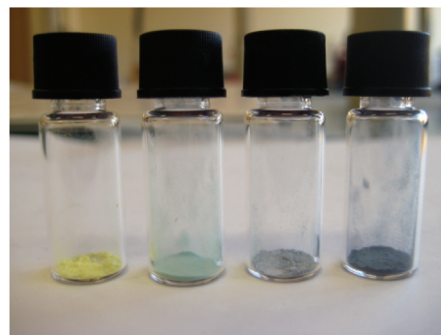

Fig. 4 Visual comparison of Zn(NDC)(DPMBI), Zn(NDC)(DPMBI)·Na$_{0.233}$, Zn(NDC)-(DPMBI)·Na$_{0.367}$ and Zn(NDC)(DPMBI)·Na$_{0.378}$ (left to right).

$Zn_2(NDC)_2(DPNI)$ which was accompanied by a colour change from yellow in the neutral material to green/brown in the monoradical species.[4] In the case of $Zn(NDC)(DPMBI) \cdot Na_{0.378}$, the initially purple solid attained a deep green colouration over a two week period (under an inert atmosphere), suggesting that charge equilibration of the neutral, monoradical and dianion mixture to the neutral and monoradical species may be occurring. Exposure of any one of the chemically reduced frameworks to air resulted in a colour change of the material to its original yellow colour, albeit with a loss of crystallinity.

Detection of the radical anion

Continuous wave X-band EPR analysis of $Zn(NDC)(DPMBI) \cdot Na_{0.233}$, $Zn(NDC)(DPMBI) \cdot Na_{0.367}$ and $Zn(NDC)(DPMBI) \cdot Na_{0.378}$ confirmed the presence of a spin-doublet arising from a single unpaired electron that corresponds to a Landé g-factor of between 2.0016 and 2.0035, close to the theoretical value for a free electron (2.0023) (ESI†).[18] Due to the diamagnetic nature of the d^{10} Zn^{2+} metal centre, the paramagnetic signal can be assigned solely to unpaired electrons on the DPMBI ligand backbone. The lack of hyperfine coupling from ^1H or ^{14}N can be attributed to the loss of spectral resolution and line broadening due to the solid state measurement on powdered samples.

Solid state Vis-NIR spectroelectrochemical (SEC) measurements on $Zn(NDC)(DPMBI)$ were employed to monitor the diffuse reflectance spectrum and colour of the material as a function of its redox state.[13] At an applied potential of −2.20 V, the initially light yellow sample attained a green colouration, as evidenced by the gradual emergence of bands in the visible region of the spectrum between $14\,000$ and $20\,000$ cm^{-1} in Fig. 5. These bands were absent in the neutral material at 0 V (black line), and are characteristic of the monoradical anion of the pyromellitic ligand core (brown line), as detailed in previous literature reports.[19] A rapid and significant increase in the intensities of the spectral bands across the visible region was observed as the potential was maintained at −2.20 V, resulting in a dark purple colouration of the material (depicted by the grey spectrum in Fig. 5, see also ESI†). The intensities of the bands continued to increase incrementally at a constant rate as the potential was further maintained at −2.20 V. A red shift of the band in the region $22\,500$–$25\,000$ cm^{-1} was also observed upon reduction of the framework.

The spectroelectrochemical data appear to be consistent with two redox processes in the framework which may be characterised as the reduction of the neutral material to the monoradical anion $Zn(NDC)(DPMBI^{\cdot -})$ as depicted by the brown spectrum in Fig. 5, followed by the reduction to the dianion $Zn(NDC)(DPMBI^{2-})$, as depicted by the grey spectrum. In comparison to the electrochemical data for $Zn(NDC)(DPMBI)$ shown in Fig. 2, a potential slightly more cathodic than that required for the second reduction process was employed in the SEC experiment due to the higher cell resistance.
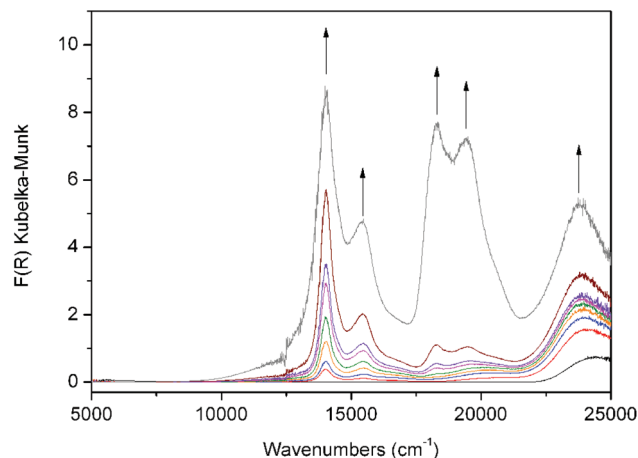

Fig. 5 Solid state Vis-NIR SEC data for $Zn(NDC)(DPMBI)$. Arrows indicate the direction of spectral changes which are accompanied by a colour change from light yellow (black line) to green (brown line) and dark purple (grey line).
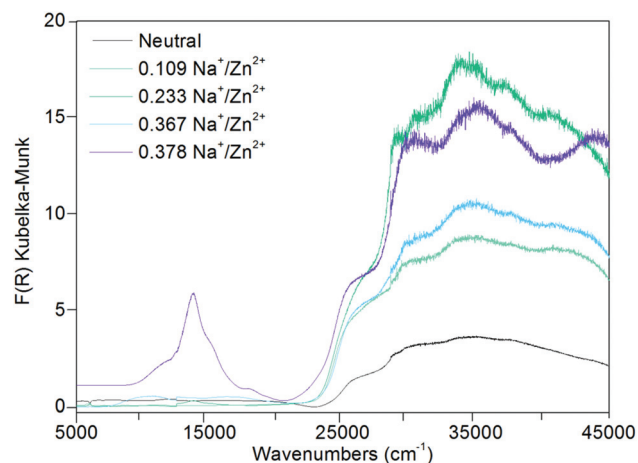

Fig. 6 Solid state UV-Vis-NIR data for $Zn(NDC)(DPMBI)$ and its reduced species.

The UV-Vis-NIR spectra for the chemically reduced frameworks $Zn(NDC)(DPMBI) \cdot Na_{0.233}$, $Zn(NDC)(DPMBI) \cdot Na_{0.367}$ and $Zn(NDC)(DPMBI) \cdot Na_{0.378}$ (Fig. 6) revealed bands in the region $12\,500$–$20\,000$ cm^{-1} which correspond to those observed for the DPMBI monoradical in Fig. 5, hence providing additional confirmation of the chemical reduction to the monoradical form. The bands occurring in the region above $27\,500$ cm^{-1} are attributed to $\pi \rightarrow \pi^*$ transitions of the pyromellitic diimide core, by comparison with the previously reported UV spectrum for the related naphthalene diimide ligand core.[13] In addition to intra-ligand transitions for the DPMBI ligands, $\pi \rightarrow \pi^*$ transitions for the NDC core provide additional contributions to the bands in the UV region above $30\,000$ cm^{-1}.

A comparison of the spectra for the chemically reduced frameworks with those observed using SEC indicates that the monoradical anion of DPMBI is present in $Zn(NDC)(DPMBI) \cdot Na_{0.378}$, with smaller amounts present in the three other reduced forms (as confirmed by EPR). There is no evidence for

the presence of the dianion form of DPMBI in even the most highly reduced system under investigation.

Gas adsorption studies

A BET surface area of 608.2 ± 0.7 m^2 g^{-1} was determined for Zn(NDC)(DPMBI) from the N$_2$ adsorption isotherm at 77 K (ESI†). Despite the high degree of catenation in the four-fold interpenetrated framework, this has not dramatically diminished the porosity of the material compared with the doubly-interpenetrated pillared paddlewheel framework Zn$_2$(NDC)$_2$-(DPNI) (DPNI = N,N'-di-(4-pyridyl)-1,4,5,8-napthalenetetracarboxydiimide), which possesses a surface area of 802 m^2 g^{-1}.[4] Chemical reduction of Zn(NDC)(DPMBI) results in a gradual decrease in the BET surface area as the concentration of Na$^+$ increases (Table 1 and ESI†). The adsorption isotherms for the neutral framework and its reduced analogues all exhibit two steps in the low pressure region (10^{-7}–10^{-4} P/P_0) which are likely to result from framework flexibility due to the methylene linkers in the DPMBI ligand.

With the exception of Zn(NDC)(DPMBI)·Na$_{0.367}$, the BET surface areas of the chemically reduced frameworks decrease as the extent of reduction and the Na$^+$ content increases. Although, extreme care was taken to treat each sample in an identical manner during the chemical reduction and activation procedures, the non-monotonic variation in surface areas with reduction may reflect a degree of sample dependence. In materials possessing one dimensional channels where pore blocking is possible, very small changes in sample activation may lead to major variations in the adsorption properties. Such deviations have been well-documented even for three dimensional frameworks such as MOF-5, where significant changes in the surface areas and adsorption properties have been observed despite identical PXRD patterns.[20]

The increased surface area for Zn(NDC)(DPMBI)·Na$_{0.367}$ relative to the neutral framework may be attributed to the aforementioned dependence on sample preparation; however in view of the identical methods employed, it is plausible that the occupation of sites between catenated nets by an optimal number of Na$^+$ ions enhances guest transport through the channels by opening up the pore accessible space. A similar explanation has been proposed recently by Hupp and co-workers for H$_2$ adsorption in the related framework Zn$_2$(NDC)$_2$(DPNI) and its reduced congeners.[4]

Gas sorption experiments under CO$_2$ and N$_2$ at 298 K were performed on the Zn(NDC)(DPMBI) framework and its

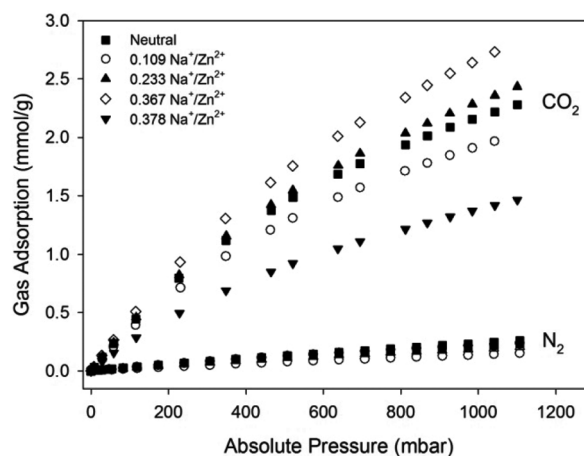**Fig. 7** CO$_2$ and N$_2$ adsorption isotherms for Zn(NDC)(DPMBI) and its reduced species at 298 K.

reduced analogues (Fig. 7, Table 1). All frameworks exhibited minimal N$_2$ uptake at 298 K, as expected due to the low polarisability of this gas molecule. The decrease in the CO$_2$ adsorption for Zn(NDC)(DPMBI)·Na$_{0.109}$ relative to the neutral framework has been attributed to a lower bulk crystallinity of the sample, as evidenced by the decreased reflection intensities in the PXRD pattern (ESI†). An improvement in the CO$_2$ uptake for Zn(NDC)(DPMBI)·Na$_{0.233}$ is observed across the 0–1 bar pressure range relative to the neutral framework, despite the reduced surface area, suggesting that the origins of the enhanced uptake are electrostatic interactions between CO$_2$ molecules and the reduced sites in the framework, as well as the interstitial alkali counter-ions. As pore blockage becomes pronounced due to an over-accumulation of Na$^+$ ions in the most highly reduced framework Zn(NDC)(DPMBI)·Na$_{0.378}$, the CO$_2$ uptake decreases relative to the neutral framework, which is consistent with the decreased BET surface area.

The sorption data indicate that CO$_2$ uptake improves up to an optimum concentration of the counter-ion; however, beyond this concentration, pore obstruction significantly hinders guest uptake.[4] In the case of Zn(NDC)(DPMBI)·Na$_{0.367}$, the increased CO$_2$ uptake appears to reflect the improved surface area relative to the neutral framework.

The CO$_2$/N$_2$ selectivity factors (S) from pure gas adsorption isotherms were calculated to be 14, 16, 18, 17 and 16 for Zn(NDC)(DPMBI), Zn(NDC)(DPMBI)·Na$_{0.109}$, Zn(NDC)(DPMBI)·Na$_{0.233}$, Zn(NDC)(DPMBI)·Na$_{0.367}$ and Zn(NDC)(DPMBI)·Na$_{0.378}$, respectively, for a binary 15% CO$_2$–85% N$_2$ mixture. In order to gain a more realistic value for selectivity in a mixed CO$_2$–N$_2$ gas system, IAST calculations were employed for a binary mixture comprised of 0.15 bar CO$_2$ and 0.85 bar N$_2$.[21] This method yielded S values of 17, 22, 21.5, 25 and 20 for Zn(NDC)(DPMBI), Zn(NDC)(DPMBI)·Na$_{0.109}$, Zn(NDC)(DPMBI)·Na$_{0.233}$, Zn(NDC)(DPMBI)·Na$_{0.367}$ and Zn(NDC)(DPMBI)·Na$_{0.378}$ at 1 bar (Fig. 8), respectively, which are larger than those obtained from pure gas adsorption isotherms. The selectivity of the reduced frameworks for CO$_2$ separation trends upwards

Table 1 BET surface areas measured at 77 K and CO$_2$ adsorption data at 298 K and 1 atm for Zn(NDC)(DPMBI) and its reduced species

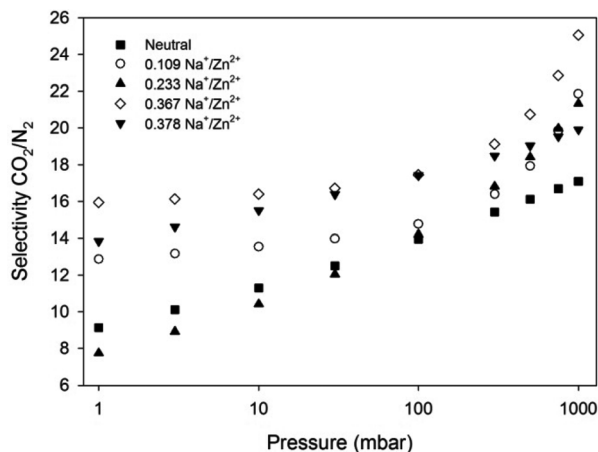| Molar ratio Na$^+$/Zn^{2+}	BET surface area (m^2 g^{-1})	CO$_2$ uptake (mmol g^{-1})
—	608.2 ± 0.7	2.23
0.109	546.2 ± 0.2	1.97
0.233	539.9 ± 0.6	2.37
0.367	653 ± 3	2.74
0.378	345.2 ± 0.1	1.42

Fig. 8 IAST predicted CO_2/N_2 selectivity based on a binary 15% CO_2–85% N_2 mixture for Zn(NDC)(DPMBI) and its reduced species at 298 K.

as the pressure approaches 1 bar, suggesting that CO_2 is more competitively adsorbed from the 15% CO_2–85% N_2 mixture. The marginal improvement in the CO_2/N_2 selectivities observed in the reduced species compared to the neutral parent framework are evidence of the stronger attractions between the CO_2 molecules and the increased electron density of the reduced DPMBI ligand backbone and the intercalated alkali cations. The debilitating effect of pore obstruction upon chemical reduction of the highly catenated framework could mitigate the accessibility of adsorption sites preferred by CO_2, and hence account for the small increase in S across the series.

A key feature of framework reduction is the enhancement of the isosteric heat of adsorption for CO_2, $|Q_{st}|$ (Fig. 9).[5] The framework Zn(NDC)(DPMBI)·Na$_{0.109}$ exhibits a higher $|Q_{st}|$ than its neutral analogue, which is further increased in Zn(NDC)-(DPMBI)·Na$_{0.233}$ and Zn(NDC)(DPMBI)·Na$_{0.378}$; this result is consistent with the hypothesised enhancement of adsorbate and adsorbent interactions.[4,8] The unexpected lowering of the
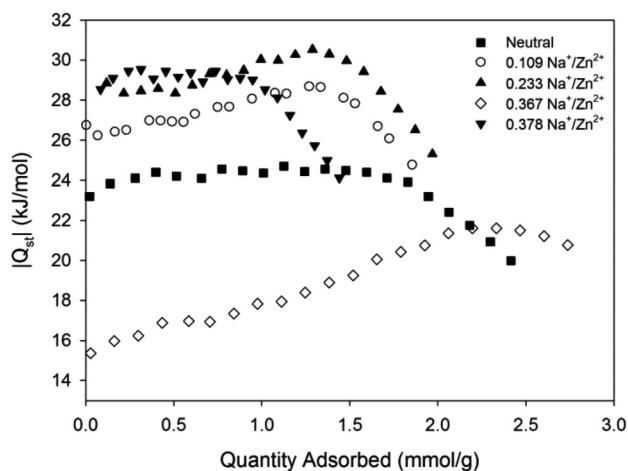
$|Q_{st}|$ in Zn(NDC)(DPMBI)·Na$_{0.367}$ and the observed increase in $|Q_{st}|$ with adsorbate loading is counterintuitive, and is tentatively ascribed to the maximal displacement of catenated frameworks resulting in multilayer formation of CO_2 (the isosteric heat of adsorption for CO_2 on itself is 17 kJ mol^{-1}). Such adsorbate–adsorbate interactions appear to dominate at low partial pressures (<1.5 mmol g^{-1}) before adsorbate–adsorbent interactions between CO_2 and the reduced framework, or intercalated alkali cations dominate the heat of adsorption profile.

The moderate enhancement in selective CO_2/N_2 sorption at pressures pertinent to post-combustion flue gas separation *via* framework reduction has been successfully demonstrated in the novel framework Zn(NDC)(DPMBI). The reasonable $|Q_{st}|$ for CO_2 (<30 kJ mol^{-1} for the neutral framework and its reduced analogues), which falls within the range for physisorption, suggests that mild activation conditions may be employed for framework regeneration *via* a pressure or temperature swing adsorption process. Alternatively, the dependence of the adsorption characteristics on the redox state of the material suggests that an alternative electrical swing adsorption process may be applicable.

Conclusions

The new porous framework Zn(NDC)(DPMBI) with a moderate surface area of 608.2 ± 0.7 m^2 g^{-1} retains its crystallinity upon chemical reduction with NaNp. With increasing Na$^+$ ion content, the CO_2 uptake of the framework is enhanced up to a molar Na$^+$/Zn^{2+} ratio of 0.367, where the CO_2 adsorption is maximised at 1 bar; beyond this dopant concentration, the CO_2 uptake is significantly lowered. The optimisation of the uptake is ascribed to maximal displacement of the four interpenetrated networks of Zn(NDC)(DPMBI) at a Na$^+$/Zn^{2+} ratio of 0.367, followed by an over-accommodation of Na$^+$ ions in the pores at higher dopant concentrations. The isosteric heat of adsorption for CO_2 and the CO_2/N_2 selectivity also increase with the extent of chemical reduction, confirming the enhancement of interactions between CO_2 and the framework or the alkali cations. The comparatively higher selectivities determined from IAST calculations compared with the estimations from pure gas adsorption isotherms suggest that CO_2 is preferentially adsorbed by the reduced frameworks from a binary CO_2–N_2 mixture.

This study further supports the promise of chemical reduction of redox-active frameworks as a potential mechanism for enhancing selective CO_2 capture from flue gas in post-combustion capture applications. Importantly, the work has also demonstrated the application of solid state Vis-NIR spectroelectrochemistry[13] for corroborating the extent of framework reduction in the doped materials. The further development and understanding of the properties of redox-active frameworks may pave the way towards more energy efficient methods of regeneration for carbon capture materials such as Electrical Swing Adsorption (ESA).

Fig. 9 CO_2 heats of adsorption for Zn(NDC)(DPMBI) and its reduced species.

Experimental section

Materials

All reagents and chemicals were commercially available and were used without purification. Sodium metal (Caution: explosive when wet) was stored under mineral oil and was washed with THF and handled under an inert Ar atmosphere.

General characterisation methods

Powder X-ray diffraction (PXRD) data were obtained using a PANalytical X'Pert PRO Diffractometer producing Cu-Kα (λ = 1.5406 Å) radiation which was equipped with a solid-state PIXcel detector. Air sensitive samples were loaded into glass capillaries under an inert Ar atmosphere which were capped with silicone grease before being flame sealed. Thermogravimetric analysis (TGA) was performed on a TA Instruments' Hi-Res TGA 2950 Thermogravimetric Analyser heating to 600 °C at a ramp rate of 2 °C min^{-1} under a flow of N_2 (0.1 L min^{-1}). Elemental Analyses were determined at the Chemical Analysis Facility at Macquarie University. Samples were dried at 110 °C for 16 hours prior to analyses which were conducted in duplicate.

Syntheses

N,N'-Di-(4-pyridylmethyl)-1,2,4,5-benzenetetracarboxydiimide (DPMBI). The procedure for the synthesis of DPMBI was adapted from the method reported for N,N'-di-(4-pyridyl)-1,2,4,5-benzenetetracarboxydiimide.[22] Under a dinitrogen atmosphere, deaerated DMF (20 mL) was added to 1,2,4,5-benzenetetracarboxylic dianhydride (1.00 g, 4.6 mmol) and 4-(aminomethyl)pyridine (1.16 mL, 10.0 mmol). The solution was refluxed for 12 h after which it was cooled in an ice bath. The resulting slurry was filtered and the isolated solid was washed with dichloromethane and acetone to yield the product as a yellow solid. Yield: 1.34 g, 3.37 mmol, 73%. m.p.: 327 °C. ^{1}H NMR (300 MHz, CF$_3$COOD): δ = 8.78 (d, J = 6.0 Hz, 4H), 8.51 (s, 2H), 8.13 (d, J = 6.0 Hz, 4H), 5.28 (s, 4H). Anal. Calcd for C$_{22}$H$_{14}$N$_4$O$_4$ (M_w = 398.40 g mol^{-1}): C 66.33, H 3.54, N 14.06. Found: C 66.28, H 3.50, N 14.14.

Zn(NDC)(DPMBI). A mixture of Zn(NO$_3$)$_2$·6H$_2$O (595 mg, 2.0 mmol), H$_2$NDC (87 mg, 0.4 mmol) and DPMBI (160 mg, 0.4 mmol) in DMF (200 mL) was heated at 80 °C with stirring for two days. A pale yellow, crystalline powder was isolated by vacuum filtration from the yellow mother liquor and washed with DMF. Yield: 217 mg, 0.32 mmol, 80% based on DPMBI. Anal. Calcd for C$_{34}$H$_{20}$N$_4$O$_8$Zn (M_w = 677.93 g mol^{-1}): C 60.23, H 2.97, N 8.27. Found: C 51.57, H 4.15, N 7.06.

Single crystal analysis of Zn(NDC)(DPMBI)·2DMF. Yellow, needle-like, prismatic crystals of Zn(NDC)(DPMBI) for single crystal X-ray diffraction analysis were obtained at one-tenth the scale of the bulk synthesis. The reagents were introduced to a 10 mL glass vial which was placed in an aluminium-lined heating block without agitation for 2 days.

A pale yellow prismatic crystal was attached with Exxon Paratone N, to a short length of fibre supported on a thin piece of copper wire inserted in a copper mounting pin. The

crystal was quenched in a cold nitrogen gas stream from an Oxford Cryosystems Cryostream. A SuperNova Dual equipped with an Atlas detector and employing mirror monochromated Cu(Kα) radiation from a micro-source was used for the data collection. Cell constants were obtained from a least squares refinement against 78 752 reflections located between 6 and 152° 2θ. Data were collected at 150(2) K with ω scans to 153° 2θ. The data processing was undertaken with CrysAlis Pro[23] and subsequent computations were carried out with WinGX[24] and ShelXle.[25] A multi-scan absorption correction was applied[23] to the data.

The structure was solved in the space group $Pbcn$(#60) by direct methods with SIR-97,[26] and extended and refined with SHELXL-97.[27] The asymmetric unit contains half of a tetrahedrally coordinated Zn complex molecule, together with two dimethylformamide solvent molecules. Tetrahedral coordination is completed by the bridging ligands of symmetry related complex molecules (*: $-x - 0.5$, $y - 0.5$, z and ': $-x + 0.5$, $-y + 0.5$, $z + 0.5$). Within the unit cell the solvent is located along four channels running parallel to the b axis and approximately located at (0.25, b, 0.4), (0.25, b, 0.9), (0.75, b, 0.1) and (0.75, b, 0.6). The non-hydrogen atom sites in the asymmetric unit were modelled with anisotropic displacement parameters and a riding atom model with group displacement parameters was used for the hydrogen atoms. An ORTEP[28,29] depiction of the material with 50% displacement ellipsoids is provided in the ESI.†

Crystal data: C$_{40}$H$_{34}$N$_6$O$_{10}$Zn$_1$, MW 824.10, space group $Pbcn$(#60), a 25.91510(10), b 14.17440(10), c 20.60420(10) Å, V 7568.56(7) Å^3, D_c 1.446 g cm^{-3}, Z 8, crystal size 0.187 × 0.177 × 0.062 mm, colour pale yellow, habit prism, temperature 150(2) K, λ(Cu Kα) 1.5418 Å, λ(Cu Kα) 1.478 mm^{-1}, $T_{min,max}$ 0.86065, 1.00000, 2θ_{max} 152.98, hkl range -32 32, -17 15, -25 25, N 182364, N_{ind} 7924(R_{merge} 0.0269), N_{obs} 7358($I > 2\sigma(I)$), N_{var} 518, residuals* $R_1(F)$ 0.0523, w$R_2(F^2)$ 0.1749, GoF(all) 1.180, $\Delta\rho_{min,max}$ -0.654, 0.891 e$^-$ Å^{-3}. *$R_1 = \Sigma||F_o| - |F_c||/\Sigma|F_o|$ for $F_o > 2\sigma(F_o)$; w$R_2 = (\Sigma w(F_o{}^2 - F_c{}^2)^2/\Sigma(wF_c{}^2)^2)^{1/2}$ all reflections w $= 1/[\sigma^2(F_o{}^2) + (0.1P)^2 + 5.0P]$ where $P = (F_o{}^2 + 2F_c{}^2)/3$.

Pore size analysis. A pore size analysis of the framework Zn(NDC)(DPMBI) was conducted using the RASPA Package from Northwestern University, USA (ESI†).[15]

Chemical reduction of Zn(NDC)(DPMBI). Sodium naphthalenide (NaNp) was prepared *via* previously reported methods.[5] Chemical reduction of Zn(NDC)(DPMBI) was performed under an inert Ar atmosphere. To a mixture of Zn(NDC)(DPMBI) in neat THF, a molar ratio equivalence of the reducing agent (0.5, 1, 1.5 and 2 molar equivalents of 0.1 M NaNp in THF) was added drop-wise with stirring. The mixture was allowed to stir for 30 min and was finally washed with two consecutive aliquots of THF (15 mL). The resultant framework was surface dried under vacuum. Extreme care was taken to treat each sample in an identical manner during the reduction procedure.

The concentrations of Na$^+$ and Zn^{2+} in the reduced MOFs were determined *via* Solution Inductively Coupled Plasma

Atomic Emission Spectroscopy (ICP-AES) at the Analytical Centre of the University of New South Wales. The framework materials were digested in high purity concentrated nitric acid, filtered to remove insoluble H_2NDC, and finally diluted to achieve an acid content below 5%. Three readings were obtained to yield an average concentration which is reported in percent weight of the sample. Yttrium was introduced online as an internal reference.

Solid state electrochemistry

Solid state cyclic voltammetry (CV) was performed using a BASi Epsilon Electrochemical Analyser with ferrocene (Fc) as an internal reference. Measurements were conducted under an inert Ar atmosphere using a conventional 3-electrode cell with a glassy carbon working electrode containing the immobilised solid, a Pt wire auxiliary electrode and an Ag/Ag^+ quasi reference electrode.

A 0.01 M tetrabutylammonium hexafluorophosphate ($[n\text{-}Bu_4N]PF_6$)/CH_3CN electrolyte was employed with a scan rate of 100 mV s^{-1}.

Solid state Vis-NIR spectroelectrochemistry (SEC)

Visible-near infrared (Vis-NIR) data were collected using a CARY5000 Spectrometer equipped with a Harrick Omni Diff Probe attachment. Electrochemical experiments were performed in a Teflon SEC cell comprising two side arms separately accommodating a platinum wire auxiliary electrode, and an Ag/Ag^+ wire quasi-reference electrode.[13] These side arms connect at a central compartment that harbours a 0.01 M $TBAPF_6$/CH_3CN electrolyte. The sample of interest was immobilised onto an Indium-Tin-Oxide (ITO) coated quartz slide (working electrode) by a strip of Teflon tape, and the circuit was completed with conductive copper tape. This slide was inverted over the central compartment to enable contact between the sample and electrolyte, and was finally fixed with adhesive tape. A baseline scan of the Teflon tape was collected from 5000–25 000 cm^{-1}. Potentials were controlled using an eDAQ e-corder 410 potentiostat. Continuous scans of the sample were undertaken at a potential of 0 V until spectral equilibration was achieved. A cathodic potential was then manually applied incrementally prior to spectral collection.

Solid state electron paramagnetic resonance (EPR)

EPR measurements were obtained using a Bruker Elexsys 500 X-Band Spectrometer equipped with a 15″ magnet with rapid scan coils. Samples were loaded into quartz capillary tubes which were sealed with a cap and parafilm under an Ar atmosphere. EPR scans were performed at room temperature with a microwave power of 0.6256 mW and a modulation frequency of 100 kHz.

Gas adsorption measurements

Pure gas adsorption measurements were conducted using a Micromeritics Accelerated Surface Area and Porosimetry System (ASAP) 2020. Approximately 50–80 mg of Zn(NDC)-(DPMBI) was degassed via a temperature program of 2 °C min^{-1}

to 80 °C followed by 1 °C min^{-1} to 140 °C where it was held for at least 6 h prior to analysis. Extreme care was taken to treat each sample in an identical manner during the activation procedure. Surface area measurements were obtained at 77 K via incremental dosing of N_2 from 0–1 bar, and the Brunauer, Emmett and Teller (BET) surface area was determined through the use of the ASAP 2020 V4.01 software. Gas adsorption measurements for N_2 were collected at 25 °C, and for CO_2 at 25, 35 and 45 °C, both over a pressure range of 0–1 bar. Ambient temperatures were regulated using a John Morris Scientific Pty Ltd Julabo F25 Circulating Heating and Cooling Unit. $|Q_{st}|$ calculations for CO_2 utilising data from 25, 35 and 45 °C CO_2 isotherms were performed using the Clausius–Clapeyron eqn (1):[3]

$$(\ln P)_N = -\left(\frac{Q_{st}}{R}\right)\left(\frac{1}{T}\right) + C \tag{1}$$

where P is pressure, N is the amount adsorbed, T is temperature, R is the universal gas constant and C is a constant.

Selectivity factor and IAST calculations

The selectivity factors (S) estimated from CO_2 and N_2 pure gas isotherms were determined according to eqn (2), where S is the selectivity factor, q is the quantity of gas adsorbed and p is the partial pressure of the gas adsorbed. Calculations assumed a flue gas composition of 15% CO_2 and 85% N_2 at 1 bar, therefore assuming zero trace impurities.[3]

$$S = \frac{q_1/q_2}{p_1/p_2} \tag{2}$$

Modelling of a binary CO_2–N_2 mixed gas system was conducted from pure gas isotherms using the Ideal Adsorbed Solution Theory (IAST).[21] Here, a single-site Langmuir–Freundlich (SSLF) equation (eqn (3)) was used to fit the pure gas adsorption isotherms of CO_2 and N_2, where P is the pressure of bulk gas at equilibrium with the adsorbed phase, $N_{A,sat}$ is the maximum loading, k_A is the affinity constant, and n_A is used to characterise the deviation from the simple Langmuir equation. The estimated flue gas composition was 15% CO_2 and 85% N_2 (assuming zero trace impurities).

$$N = \frac{N_{A,sat} k_A P^{n_A}}{1 + k_A P^{n_A}} \tag{3}$$

The fitted parameters were then used to predict the adsorption of the binary mixture. Different models were freely applied to fit the adsorption isotherm in order to fit the data over the pressure range of interest.

Acknowledgements

Notes and references

1 C. J. Kepert, in *Porous Materials*, John Wiley & Sons Ltd, 2010, pp. 1–67.

2 D. M. D'Alessandro, B. Smit and J. R. Long, *Angew. Chem., Int. Ed.*, 2010, **49**, 6058–6082.

3 K. Sumida, D. L. Rogow, J. A. Mason, T. M. McDonald, E. D. Bloch, Z. R. Herm, T.-H. Bae and J. R. Long, *Chem. Rev.*, 2011, **112**, 724–781.

4 K. L. Mulfort and J. T. Hupp, *Inorg. Chem.*, 2008, **47**, 7936–7938.

5 K. L. Mulfort, T. M. Wilson, M. R. Wasielewski and J. T. Hupp, *Langmuir*, 2009, **25**, 503–508.

6 K. L. Mulfort and J. T. Hupp, *J. Am. Chem. Soc.*, 2007, **129**, 9604–9605.

7 Y.-S. Bae, B. G. Hauser, O. K. Farha, J. T. Hupp and R. Q. Snurr, *Microporous Mesoporous Mater.*, 2011, **141**, 231–235.

8 H. J. Park and M. P. Suh, *Chem. Sci.*, 2013, **4**, 685–690.

9 S.-i. Kato, Y. Nonaka, T. Shimasaki, K. Goto and T. Shinmyozu, *J. Org. Chem.*, 2008, **73**, 4063–4075.

10 S.-i. Kato, T. Matsumoto, K. Ideta, T. Shimasaki, K. Goto and T. Shinmyozu, *J. Org. Chem.*, 2006, **71**, 4723–4733.

11 M. Pan, X.-M. Lin, G.-B. Li and C.-Y. Su, *Coord. Chem. Rev.*, 2011, **255**, 1921–1936.

12 D. M. D'Alessandro, J. R. R. Kanga and J. S. Caddy, *Aust. J. Chem.*, 2011, **64**, 718–722.

13 P. M. Usov, C. Fabian and D. M. D'Alessandro, *Chem. Commun.*, 2012, **48**, 3945–3947.

14 N. Stock and S. Biswas, *Chem. Rev.*, 2011, **112**, 933–969.

15 D. Dubbeldam, S. Calero, D. E. Ellis and R. Q. Snurr, *RASPA 1.0*, Northwestern University, Evanston, 2008.

16 D. G. Hamilton, M. Montalti, L. Prodi, M. Fontani, P. Zanello and J. K. M. Sanders, *Chem.–Eur. J.*, 2000, **6**, 608–617.

17 N. G. Connelly and W. E. Geiger, *Chem. Rev.*, 1996, **96**, 877–910.

18 D. F. Shriver, P. W. Atkins and C. H. Langford, *Inorganic Chemistry*, Oxford University Press, Oxford, 1990.

19 T. Andruniow and M. Pawlikowski, *Chem. Phys. Lett.*, 2000, **321**, 485–490.

20 S. S. Kaye, A. Dailly, O. M. Yaghi and J. R. Long, *J. Am. Chem. Soc.*, 2007, **129**, 14176–14177.

21 A. L. Myers and J. M. Prausnitz, *AIChE J.*, 1965, **11**, 121–127.

22 P. H. Dinolfo, M. E. Williams, C. L. Stern and J. T. Hupp, *J. Am. Chem. Soc.*, 2004, **126**, 12989–13001.

23 A. Technologies, *CrysAlisPro Version 1.171.35.11*, released 16-05-2011.

24 L. J. Farrugia, *J. Appl. Crystallogr.*, 1999, **32**, 837–838.

25 C. B. Hübschle, G. M. Sheldrick and B. Dittrich, *J. Appl. Crystallogr.*, 2011, **44**, 1281–1284.

26 A. Altomare, M. C. Burla, M. Camalli, G. L. Cascarano, C. Giacovazzo, A. Guagliardi, A. G. G. Moliterni, G. Polidori and R. Spagna, *J. Appl. Crystallogr.*, 1998, **32**, 115–119.

27 G. M. Sheldrick, *SHELX97 Programs for Crystal Structure Analysis*, Tammanstrasse 4, D-3400 Göttingen, Germany, 1998.

28 C. K. Johnson, ORTEPII. Report ORNL-5138, Oak Ridge National Laboratory, Oak Ridge, Tennessee, 1976.

29 S. R. Hall, D. J. du Boulay and R. Olthof-Hazekamp, *Xtal3.6 System*, University of Western Australia, Perth, 1999.